Nanotechnology in Biomaterials

JOURNAL OF
biomaterials
applications

Journal of Biomaterials Applications
2025, Vol. 40(1) 145–162

DOI: 10.1177/08853282251327486
journals.sagepub.com/home/jba
Sage

Making vancomycin a potent broad-spectrum antimicrobial agent using polyaziridine-stabilized gold nanoparticles as a delivery vehicle

Atul Kumar Tiwari[1], Aishwarya Nikhil[2], Avinash Chaurasia[3], Prem C. Pandey[1], Roger J. Narayan[4] and Munesh Kumar Gupta[2]

Abstract

The rise of antimicrobial drug resistance among microorganisms presents a global challenge to clinicians. Therefore, it is essential to investigate drug delivery systems to combat resistant bacteria and fungi. This study examined the potential and mode of action of vancomycin-conjugated gold nanoparticles (PEI-AuNP@Van) to enhance vancomycin's biocidal activity against *C. tropicalis, C. albicans, E. coli*, and *P. aeruginosa*. Drug conjugation and nanoparticle characterization were assessed using UV-Vis spectroscopy, X-ray diffraction, TEM, ATR-FTIR, and fluorescence spectroscopy. Effective vancomycin conjugation on polyethyleneimine-stabilized gold nanoparticles was achieved via electrostatic interactions or hydrogen bonding between the COO-/OH groups of vancomycin and the NH- groups of polyethyleneimine, yielding nanoparticles with a narrow size distribution and high zeta potential. The high luminescence of the nanoparticles facilitated their detection in microbial cells. PEI-AuNP@Van was internalized in *C. albicans* and *C. tropicalis* but showed surface adsorption in *E. coli* and *P. aeruginosa*. The in vitro results indicated that the nanodelivery system exhibited superior biocidal activity against the tested strains compared to free vancomycin and unconjugated AuNPs. The mode of action of PEI-AuNP@Van was cell-type-dependent, involving intracellular reactive oxygen species accumulation, cell membrane integrity loss, and apoptosis. The development of antimicrobial nanoformulations using AuNPs and efficient conjugation systems offers a promising approach to address antimicrobial drug resistance.

Keywords

Vancomycin, drug delivery, gold nanoparticles, cellular localization, antimicrobial, ESKAPE

Introduction

Human diseases associated with microorganisms (e.g., bacteria, fungi, parasites, and viruses) typically respond to the administration of antimicrobial agents. However, emerging drug resistance among microorganisms, particularly *Candida* spp. And Gram-negative bacteria, poses a major global health challenge. Drug-resistant microbial infections are associated with increased mortality and substantial medical costs among hospitalized patients.[1,2] For example, the high mortality rates among those with *Candida* species infections are attributed to invasive systemic infections and septicemia, particularly in immunocompromised individuals.[1–3] *Candida* species (e.g., *C. albicans, C. parapsilosis, C. tropicalis, C. glabrata*,

[1]Department of Chemistry, Indian Institute of Technology (BHU), Varanasi, India
[2]Mycology research group, Department of Microbiology, Institute of Medical Sciences, Banaras Hindu University, Varanasi, India
[3]Department of Biotechnology, Institute of Sciences, Banaras Hindu University, Varanasi, India
[4]Joint Department of Biomedical Engineering, University of North Carolina, Chapel Hill, NC, USA

Corresponding authors:
Roger J. Narayan, Joint Department of Biomedical Engineering, University of North Carolina, Chapel Hill, NC, USA.
Email: roger_narayan@unc.edu

Munesh Kumar Gupta, Mycology research group, Department of Microbiology, Institute of Medical Sciences, Banaras Hindu University, Varanasi, India.
Email: muneshg.micro@bhu.ac.in

and *C. krusei*) inhabit healthy hosts but cause invasive infections when host immunity is compromised.[4] Despite the availability of antifungal treatments, *Candida* infection mortality rates remain high, at 45%.[5] The long-term use of azole drugs has led to increased antifungal resistance in *Candida* spp.[6] In 2019, the WHO reported approximately 4.95 million deaths related to antimicrobial-resistant (AMR) bacteria, primarily from the ESKAPE pathogens (*S. aureus, S. pneumoniae, E. coli, K. pneumoniae*, *A. baumannii*, and *P. aeruginosa*).[7] The rapid emergence of multidrug resistance (MDR) in Gram-negative bacteria severely threatens public health[8,9]; bacteria known as "superbugs" resist nearly all antibiotics and are prevalent in medical settings; this phenomenon severely limits treatment options for severe cases.

Nanotechnology may be used for addressing communicable and non-communicable diseases; for example, nanoparticles may be used as drug carriers. The physicochemical characteristics of nanoparticles (e.g., shape, surface chemistry, and size) can be modulated; as such, nanoparticles are versatile materials for combating bacterial and fungal infections.[10,11] Due to their high drug-loading capacity and capability for crossing biological membranes, surface-modified nanoparticles are excellent drug carriers.[12,13] Various metal nanoparticles and their oxides (e.g., silver, gold, aluminum oxide, zinc oxide, titanium dioxide, and copper oxide) have been extensively assessed, either alone or in combination with antibiotics or other functional molecules, with regard to their potential in treating infections.[14–17] Gold nanoparticles (AuNPs) have garnered significant attention because of their biocompatibility, optical properties, and ability to be surface-modified with specific drugs.[18] Recent studies have successfully demonstrated AuNPs as carriers for the delivery of antimicrobial agents.[19–24] Additionally, the high volume-surface ratio observed in AuNPs allows for substantial drug loading and efficient delivery to infection sites.

Mu et al. demonstrated that Ag@Au bimetallic core cell NPs that were loaded with ciprofloxacin exhibited enhanced antibacterial activity against *Escherichia coli*.[25] Similarly, Shaker et al. evaluated carbapenem-conjugated gold nanoparticles (meropenem and imipenem) against *K. pneumoniae, P. mirabilis*, and *A. baumannii*. Nanoparticles showed loading efficiencies of 72% for imipenem and 74% for meropenem. Imipenem-loaded nanoparticles reduced the minimum inhibitory concentration (MIC) fourfold; meropenem-loaded nanoparticles reduced the MIC threefold.[26] Other studies have also enhanced antibacterial drug efficacy using AuNPs as a drug carrier. Hagbani et al. used vancomycin-functionalized gold nanoparticles (V-GNPs) for treating bacterial infections.[10] The loading efficiency that was noted for vancomycin onto V-GNPs was 86.2%; the antibacterial activity of vancomycin-loaded V-GNPs was 1.4- to 1.8-fold higher against Gram-negative *E. coli*, *K. oxytoca*, and *P. aeruginosa*, and Gram-positive *S. aureus* in comparison to pure vancomycin.[10] Various strategies have been employed to improve antifungal efficacy via the conjugation of drugs or small molecules. For instance, the anti-*Candida* effects of indolicidin were compared with those of a host defense peptide that was conjugated with gold nanoparticles against fluconazole-resistant *C. albicans* isolates.[27] Numerous studies support the use of antibacterial and antifungal agents. Hsu et al. described the antifungal properties of polymyxin B, a cationic lipid oligopeptide typically utilized for the treatment of Gram-negative bacterial infections against *Fusarium* spp.[28] Similarly, Zhai et al. considered the anti-cryptococcal activity of polymyxin B.[29] Other antifungal agents have also been examined for efficacy against various fungal species. In addition, antifungal agents (e.g., caspofungin) have been evaluated for their bactericidal activity against vancomycin-resistant *E. faecium*. Thus, exploration of antibacterial agents against drug-resistant fungal isolates is warranted. This study considers the synthesis and enhancement of the in vitro antimicrobial activity of highly stable vancomycin-conjugated gold nanoparticles against *C. albicans, C. tropicalis*, and the Gram-negative bacteria *E. coli and P. aeruginosa*. Vancomycin, a known antibiotic for treating Gram-positive bacterial infections among terminally ill ICU patients, is a glycopeptide that exhibits a unique mode of action that inhibits the second stage of cell wall synthesis within bacteria.[30] However, Gram-negative bacteria resist vancomycin interaction with specific C-terminal peptides because of their outer lipopolysaccharide (LPS) membrane, which prevents drug access.[31] Therefore, this study explored the stabilization of gold nanoparticles using polyethyleneimine (PEI), a cationic polymer used for delivering nucleic acids and genes to mammalian cells, with vancomycin as a payload. This study suggests a method to combat antimicrobial drug resistance through rational conjugation and site-specific delivery of classical antibacterial and broad-spectrum biocidal agents.

Experimental section

Material and methods

All of the reagents and the materials were of analytical quality. Vancomycin, chloroauric acid trihydrate, polyethyleneimine, amphotericin B, and meropenem were purchased from Sigma Aldrich (Mumbai, India). Microbial cultures and SDA (Sabouraud dextrose agar) were obtained from RPMI (Roswell Park Memorial Institute, Buffalo, NY, USA); Mueller Hinton agar (MHA) and Mueller Hinton broth (MHB) were acquired from Hi-Media Laboratories Limited (Mumbai, India). The solvents were obtained from Merck Life Science Private Limited (Bangalore, Karnataka,

India). Other required glassware and plastic wares were purchased from Tarson Products Private Limited (Kolkata, West Bengal, India). All of the experiments were conducted in ultra-purified HPLC-grade water.

Microbial strains and growth condition

In this study, we used the ATCC strains of *C. tropicalis* (ATCC 750), *E. coli* (ATCC 25,922), *C. albicans* (ATCC 90,028), and *P. aeruginosa* (ATCC 27,853). The microbial strains were identified via conventional microbiological procedures, including morphological and cultural characteristics; pure strains were subcultured on MHA for bacterial stains and SD agar slants for fungus and stored at −20°C for further experiments.

Synthesis of colloidal vancomycin-conjugated gold nanoparticles

The vancomycin-conjugated colloidal gold nanoparticles were synthesized and described recently by Tiwari et al.[32,33] Briefly, 200 µL (10 mM, $HAuCl_4.3H_2O$) was combined with an aqueous solution (40 µL, 2 mg/mL) of vancomycin within a glass vial; this step was followed via continuous stirring for 5–10 min using a magnetic stirrer. Immediately, an aqueous solution (30 µL of 4 mg/mL, mw. 60,000 Da.) of PEI (polyethyleneimine) was added; this step was followed by the addition of 30 µL of formaldehyde (35% w/v). The reaction mixture was stirred for 40–60 min at room temperature, which resulted in the dark red-pink color that was observed in PEI-AuNP@Van.

Physical characterization of prepared nanoparticles

The synthesized PEI-AuNP@Van was characterized using a U-2900 UV-Vis spectroscopy instrument (Hitachi, Tokyo, Japan) and transmission electron microscopy (TEM; FEI Tecnai G2 20 S Twin, Hillsboro, Oregon, USA). Nanoparticle size was analyzed using ImageJ software (NIH, Bethesda, MD, USA), and data were plotted with Origin 8.5 software (Northampton, MA, USA). Dynamic light scattering (DLS) and zeta potential measurements were undertaken using a Malvern Nano Zeta Sizer (Malvern, UK). X-ray diffraction (XRD) was performed using a Rigaku Mini-Flex 600 (Tokyo, Japan) on a nanoparticle film on a silicate glass slide covering 10–80° 2θ. The fluorescence emission spectra in water were recorded using a Hitachi F7000 spectrophotometer (Tokyo, Japan). Atomic force microscopy (AFM) measurements were conducted on nanostructured films of colloidal gold nanoparticles on silanized glass plates using a Bruker Dimension Edge AFM in tapping mode at ambient conditions. Attenuated total reflectance-Fourier transform infrared (ATR-FTIR) spectroscopy was utilized to analyze conformational changes upon vancomycin loading onto PEI-AuNPs with a Nicolet iS5 spectrometer (Thermo Electron Scientific Instruments, Waltham, MA, USA), and spectra were obtained with 4 cm^{-1} resolution from 4000 to 400 cm^{-1}.

Minimal inhibitory concentration (MIC) determination

In vitro minimum inhibitory concentration (MIC) of PEI-AuNP (unconjugated) and PEI-AuNP@Van against strains of *C. tropicalis* (ATCC 750), *E. coli* (ATCC 25,922), *C. albicans* (ATCC 90,028), and *P. aeruginosa* (ATCC 27,853) were determined using a serial dilution (in purified water) technique in a sterile 96-well microtiter plate as previously described.[34,35] A 50 µg/mL PEI-AuNP@Van aqueous suspension was prepared; 100 µL was dispensed into the first well and then serially diluted to final concentrations ranging from 0.38 to 50 µg/mL. The positive controls (amphotericin B and meropenem at 32 µg/mL) and a negative control (distilled water) were similarly diluted. Each well received 100 µL of freshly prepared microbial culture; the plate was then incubated statically at 37°C for 24 h. Further, a 10-µL aliquot from each well was then subcultured on MHA (bacteria) and SD agar plates (fungal strains) for 24 h, and microbial growth was observed. MIC values corresponded to the PEI-AuNP@Van concentration that inhibited or slowed growth when compared to the control.

Microbial cell viability assay

The viability of PEI-AuNP (unconjugated) and PEI-AuNP@Van-exposed *C. albicans*, *C. tropicalis*, *E. coli*, and *P. aeruginosa* cells was assessed using propidium iodide (PI), a membrane-impermeable dye as previously described by Yadav et.al..[36] Briefly, freshly grown bacterial and fungal cultures were washed in PBS (100 mM, pH 7.2) followed by resuspension in MHB (for bacteria) and RPMI-1640 (for fungal strains); this step was followed by treatment with PEI-AuNP and PEI-AuNP@Van at their respective MIC, along with positive and growth controls, and incubation for 4 h at 37°C. Aliquots were withdrawn from each tube and then centrifuged at 3500 r/min for 5 min, followed by repeated washing and resuspension in PBS. The cells were stained with 10 µL of PI (1 mg/mL stock; λex/em = 535/617 nm), incubated at room temperature in the dark for 30 min, and then washed with PBS to remove excess dye. The treated cells were evaluated under an SP5 AOBS Super-resolution laser-scanning confocal microscope (Leica, Wetzlar, Germany) with a 40X oil immersion objective.

Determination of post-treatment dead population

To understand the percentage of dead cells after exposure to PEI-AuNP (unconjugated) and PEI-AuNP@Van, freshly grown cultures of *C. albicans*, *C. tropicalis*, *E. coli*, and *P. aeruginosa* were prepared. A 5 mL culture (10^7 CFU/mL for bacteria and 10^5 CFU/mL for fungi) in MHB and RPMI-1640 medium, respectively, received PEI-AuNP and PEI-AuNP@Van at their respective MICs. Each tube was subsequently incubated at 37°C for 4 h. Post-incubation, 2 mL aliquots were pelleted at 3500 r/min for 5 min and washed with PBS (100 mM, pH 7.2). PEI-AuNP@Van-exposed cells were stained with PI (10 µL; 1 mg/mL) and incubated in the dark for 30 min at room temperature. The stained cells were washed with PBS to remove the excess stain. The data acquisition was undertaken using BD FACSAria Fusion Flow cytometry (BD Biosciences, Franklin Lakes, NJ, USA) and BD Accuri C6 software, with measurements obtained using 20 mW laser illumination (λ = 488 nm). The assays were performed at a low sample rate (14 µL min^{-1}), with 10^4 events for fungi and 10^6 events for bacteria, and were measured logarithmically.

Endogenous ROS accumulation study

PEI-AuNP@Van-treated *C. albicans*, *C. tropicalis*, *E. coli*, and *P. aeruginosa* cells were assessed for endogenous reactive oxygen species (ROS) production after 4 h. Flow cytometry with 2′, 7′-dichlorofluorescein-diacetate (DCFH-DA) as a ROS marker was employed for the measurements.[37] The cultures were exposed to MIC values, washed with PBS (100 mM, pH 7.2), and adjusted to 10^8 CFU/mL for bacteria and 10^6 CFU/mL for fungi. Cell suspensions were incubated with 5 µM DCFH-DA for 30 min, followed by BD FACSAria Fusion Flow cytometry analysis (BD Biosciences, Franklin Lakes, NJ, USA). Data analysis was performed using BD Accuri C6 software based on light scatter and fluorescence signals from 20 mW laser illumination (λ = 488 nm). Measurements were made logarithmically; measurements were obtained at a low sample rate (14 µL/min^{-1}), with 10^4 events for fungal cells and 10^6 events for bacteria.

Phosphatidylserine externalization (apoptosis) assay

Freshly harvested (log phase) cells of the aforementioned strains were treated with PEI-AuNP@Van at their respective MICs at 37°C for 4 h; this step was followed by washing with PBS (100 mM, pH 7.2) and incubation for the next 20 min in an annexin V binding buffer that contained 5 µL/mL of Annexin V-FITC and 2 µL/mL of PI (FITC-annexin V apoptosis detection kit (BD Pharmingen™, Franklin Lakes, NJ, USA)) along with the untreated control. Further, recovered cells were visualized using an SP5 AOBS super-resolution laser-scanning confocal microscope (Leica, Wetzlar, Germany) with a 40X oil immersion objective lenses.

Raman spectroscopic studies of treated cells

Raman spectroscopy was undertaken to understand any bimolecular changes in microbial cells after exposure with PEI-AuNP@Van along with drug and growth control cells of *C. albicans*, *C. tropicalis*, *E. coli*, and *P. aeruginosa* cells. The exposed cells were pelleted and then washed twice with PBS to remove any debris. Then, the sample was placed on a microscopic glass slide and then dried under ambient conditions for 30 min. Raman measurements were obtained using a WI-Tec alpha 300 RA/S instrument (WI-Tec GmbH, Berlin, Germany). The excitation source was a Nd: YAG laser (λ = 532 nm), which provided a maximum power output of 40 mW. The laser power attenuated to ~16 mW at the sampling point. The dispersed intensity of light associated with the signal from the grating was studied with a Peltier-cooled charge-coupled device (CCD); the spectra were recorded over the range of 400-2400 cm^{-1}.

Multivariate data analysis

Principal Component Analysis (PCA) is an unsupervised technique that was used to examine spectral datasets and identify the primary patterns of variability within the spectral matrix of various samples. This method transformed correlated variables into uncorrelated ones, termed PC scores, which preserved the variability in the spectral data and eliminated random noise. The initial PC accounted for the majority of the variation that was observed in the spectral data; subsequent PCs elucidated the remaining variability.[38] While PCA is effective in revealing clusters within datasets, other biological factors with less significance, such as spectral characteristics unrelated to pathological conditions, may influence the data distribution in scatter plots. Consequently, to achieve enhanced discrimination, a supervised constraint was introduced to PCA, which placed greater emphasis on the underlying spectral information in the classification process.[39] The PCA analysis was performed using Origin 2018 software (Origin Lab. Corp, Northampton, MA, USA).

Ultra-structural visualization (Transmission electron microscopy) studies

For the transmission Electron Microscopy (TEM) (G2 20 S Twin Technai, FEI instrument, Hillsboro, OR, USA) studies, freshly harvested cells of *C. albicans, C. tropicalis, E. coli*, and *P. aeruginosa* were prepared and treated with PEI-AuNP@Van at their respective MICs and then incubated for 4 h at 37°C. After that, the culture was pelleted

down, washed with PBS, and fixed with Karnowasky solution (2% paraformaldehyde, 2.5% glutaraldehyde) in 0.1 M sodium phosphate buffer (pH 7.4) for 1 h. Further, the treated samples and control samples were drop cast onto a carbon-coated copper grid with a mess size of 300, dried for 1 h under ambient conditions, and visualized.

Cytotoxicity evaluation of PEI-AuNP@Van on HEK-293 cell line

In order to understand the toxic effects of PEI-AuNP@Van on cells, human embryonic kidney (HEK-293) cells were cultured in DMEM supplemented with 10% FBS and 1% antibiotics (Penicillin/Streptomycin). Cells were incubated at 37°C in a humidified environment with 5% CO_2 (Thermo Scientific Heracellvios 160i CO_2 incubator). A total of 10,000 cells were seeded into each well of 96-well tissue culture plates and then left overnight. On the following day, the medium was replaced with 200 µL of the fresh culture medium that contained varying concentrations of PEI-AuNP@Van (5–100 µg/mL); the cytotoxicity was examined after 24 h. Following exposure, a 5 mg mL^{-1} solution of 3-(4,5-dimethylthiazol-2-yl)-2,5-diphenyl tetrazolium bromide (MTT) in PBS pH 7.2) was added and incubated for 3 h at 37°C. The medium was then removed, and the resulting formazan crystals were solubilized in 100 µL of DMSO. After 20 min, the absorbance of the solution was evaluated at λ:570 nm with a microplate reader. The cell viability value was described as a percentage (%) relative to untreated cells using the formula as follows:

$$Cell\ viability = \frac{O.D.\ of\ treated\ cells}{O.D.\ of\ untreated\ cells} \times 100$$

Statistical analysis

All of the experiments were conducted three independent times. The data were represented in mean ± standard deviation (SD) format. The statistical significance was evaluated with ordinary one-way ANOVA tests. In this study, the p values <0.05, <0.01, and <0.001 were noted to indicate the statistical significance.

Results

Synthesis and characterization of vancomycin-conjugated gold nanoparticles

Tiwari et al. (2023) optimized a one-pot procedure for synthesizing vancomycin-conjugated AuNPs.[32,33] The resulting PEI-AuNP@Van nanoparticles exhibited an absorption maximum at 520 nm, with vancomycin interactions evaluated using UV-Vis spectrometry (Figure 1(a)). These spherical nanoparticles had a uniform size distribution, with an average diameter of 7.5 nm and a standard deviation of 0.5 nm. The smallest particle measured 3 nm, and the largest measured 12 nm (Figure 1(b) and (d)). Zeta potential analysis (Figure 1(c)) showed a sharp bimodal distribution around 48 mV, indicating a positive charge and stable dispersibility over several months. X-ray diffractometry data (2θ = 10°-80°) revealed peaks at 38.4°, 44.6°, 64.6°, and 77.7°, corresponding to hkl values of (111), (200), (220), and (311), indicating that the particles were face-centered cubic (FCC) crystalline (Figure 1(e)). AFM results (Figure 1(f)) agree with the TEM observations (Figure 1(a) and (b)).

ATR-FTIR spectroscopy was used to analyze vancomycin conjugation on PEI-AuNPs, providing semi-quantitative data that are challenging to obtain via UV-visible spectrometry. Figure 2 shows the spectra of pure vancomycin, PEI-AuNPs, and PEI-AuNP@Van. Pure vancomycin exhibited peaks at 3313 cm^{-1} (O–H stretching), 2918 cm^{-1} (C–H stretching), 2110 cm^{-1} (C≡C stretching), 1635 cm^{-1} (C = O stretching), 1435 cm^{-1} (O–H bending), 1383 cm^{-1} (C = C stretching), 1244 cm^{-1} (C–N stretching), and 1194 cm^{-1} (C–O stretching), with a strong peak at 1024 cm^{-1} (C–N/O–H stretching) (Figure 2, black line). Unconjugated AuNPs (PEI-AuNPs) exhibited peaks at 3313 cm^{-1} (O–H stretching), 1635 cm^{-1} (C = O stretching), and 1231 cm^{-1} (C–N stretching) (Figure 2, red line). Vancomycin-conjugated AuNPs (PEI-AuNP@Van) exhibited shifts and new peaks, such as 2843 cm^{-1} (C-H stretching), weakening at 1435 cm^{-1} (O–H bending), and 1115 cm^{-1} (C–O stretching of the secondary alcohol), with a shift from 1024 to 1015 cm^{-1} (C–OH stretching) (Figure 2, blue line), confirming the presence of vancomycin on the PEI-AuNP surface.

PEI-AuNP@Van nanoparticles have potent antimicrobial activity

The antimicrobial activity of PEI-AuNP@Van was examined by MIC studies that used a broth micro-dilution methodology. The results demonstrated that PEI-AuNP@Van possessed excellent antimicrobial activity against *Candida* species, *E. coli*, and *P. aeruginosa*. The determined MIC of PEI-AuNP@Van were 4.8 ± 0.68, 1.2 ± 0.59, 2.5 ± 0.91 and 4.81 ± 1.02 µg/mL, against *C. albicans*, *C. tropicalis*, *E. coli*, and *P. aeruginosa*, respectively, as shown in Table 1. Similarly, PEI-AuNPs exhibited higher MIC values than PEI-AuNP@Van; however, free vancomycin did not exhibit antimicrobial activity (Table 1).

Cell membrane integrity was compromised by PEI-AuNP@Van

When PEI-AuNP@Van encountered microbial cells, it bound to a specific site on the cell surface, resulting in

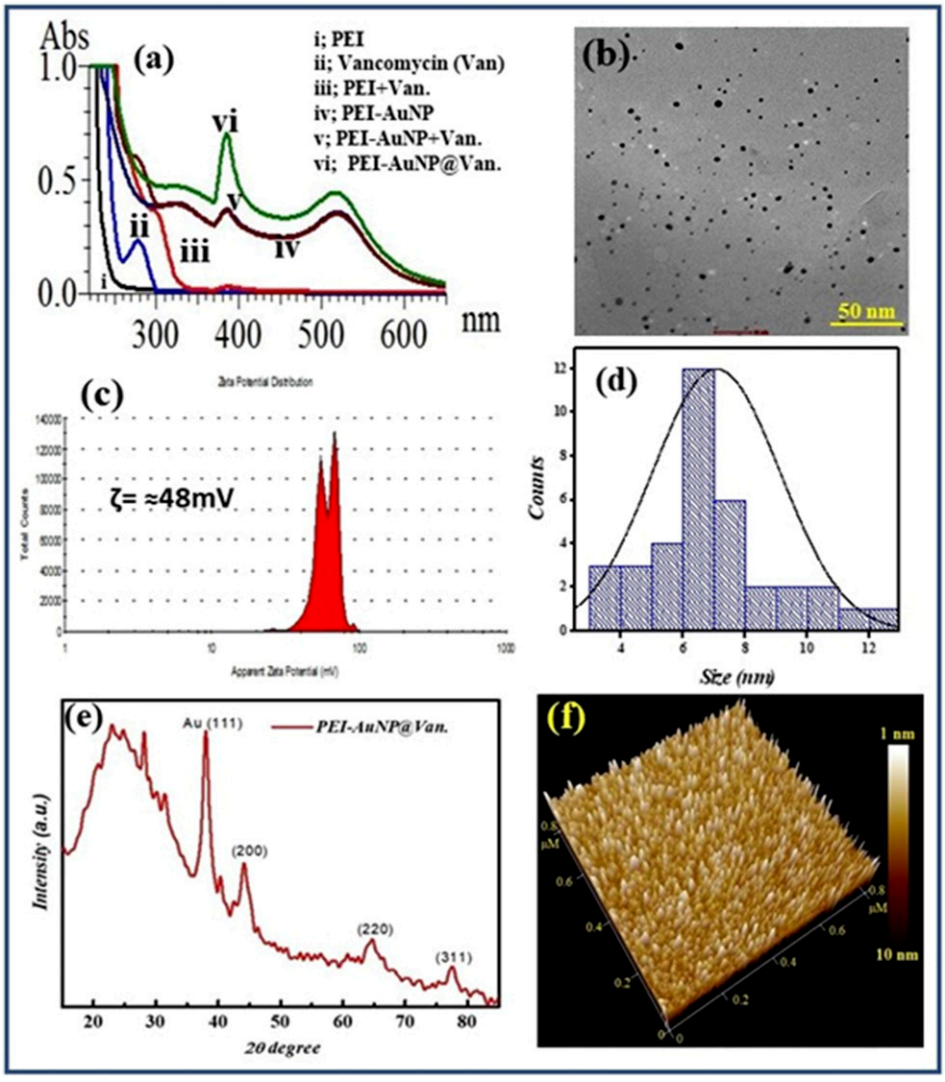

Figure 1. Physical characteristics of as-prepared vancomycin-conjugated nanoparticles (PEI-AuNP@Van). (a) UV–visible spectrum, (b) TEM micrograph, (c) zeta potential distribution, (d) particle size distribution plot, (e) X-ray diffractogram, and (f) AFM micrograph of nanoparticles. (Fig 1 (a, d and e) Adopted from ref. 33).

antimicrobial activity. As a fluorescent nanoparticle, PEI-AuNP@Van could be detected using specific excitation/emission ranges under confocal microscopy. As shown in Figure 3(a)–(h), PEI-AuNP@Van nanoparticles localized intracellularly in *C. albicans* and *C. tropicalis* cells, but adsorbed onto the cell surface of *E. coli* and *P. aeruginosa* after 4 h of exposure (Supplement Figure S1). A viability assay with propidium iodide dye (Figure 4) confirmed that PEI-AuNP@Van compromised the membranes of the treated cells. The percentage of dead cells was assessed via fluorescence-activated cell sorting with propidium iodide (PI) dye (Figure 5 and Supplement Figure S3), showing significant membrane compromise in *C. albicans* (16.3%), *C. tropicalis* (91.8%), *E. coli* (12%), and *P. aeruginosa* (85.8%). Unconjugated PEI-AuNPs showed a relatively low killing activity (Figure 5), whereas the standard antimicrobial drug exhibited excellent cell membrane-damaging behavior.

PEI-AuNP@Van induces endogenous ROS accumulation and apoptotic features in a cell type-dependent manner

Endogenous ROS generation was monitored via flow cytometry using an active dye, 2, 7 dichlorofluorescein diacetate (DCFH-DA). Interestingly, the results indicated differences in the intracellular ROS accumulation profile in the PEI-AuNP@Van exposed strains (Figure 6 and Supplement Figure S3). Compared with the

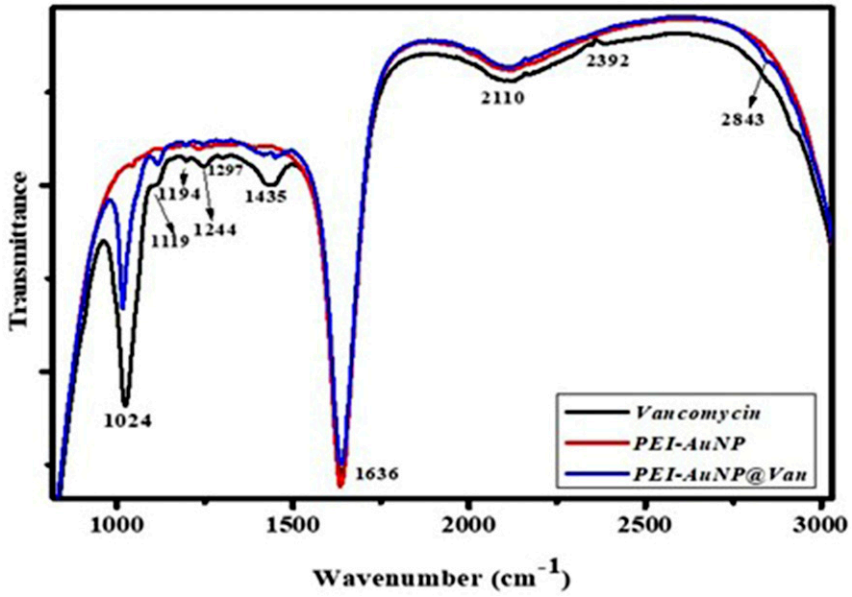

Figure 2. (a) ATR-FTIR spectra of free vancomycin (black line), unconjugated PEI-AuNPs (red line), and vancomycin-conjugated PEI-AuNPs (PEI-AuNP@Van; blue line).

Table 1. MIC values of vancomycin conjugated and unconjugated AuNPs.

	MIC (μg/mL)			
Microbial strains	Positive control (amphotericin B and meropenem were used for *Candida* spp. And Gram-negative bacterial strains, respectively)	Free vancomycin	PEI-AuNP	PEI-AuNP@Van
C albicans	1.5 ± 0.25	Not active	8.8 ± 2.3	4.8 ± 0.68
C. tropicalis	0.46 ± 0.21	Not active	4.3 ± 1.06	1.2 ± 0.59
E. coli	0.62 ± 0.57	Not active	7.89 ± 1.6	2.5 ± 0.91
P. aeruginosa	*1.5 ± 0.42*	Not active	5.23 ± 0.93	4.81 ± 1.02

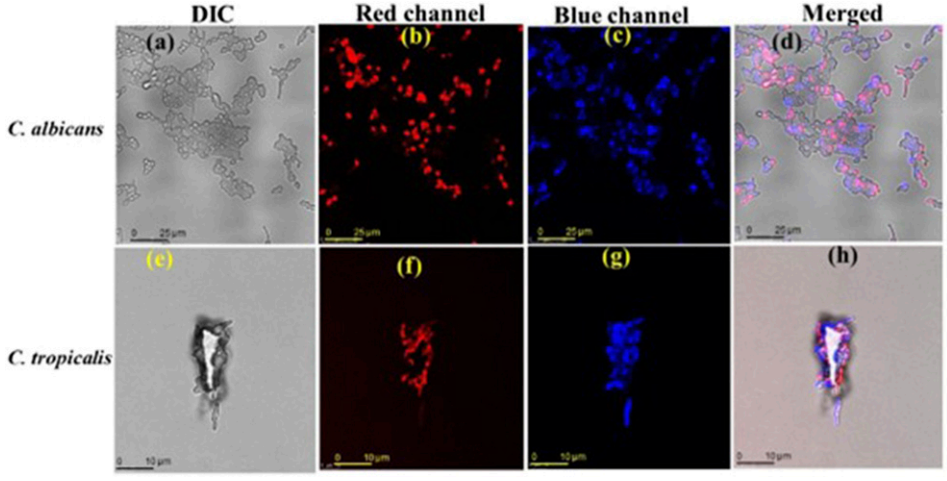

Figure 3. Confocal micrographs of the post-exposure localization of PEI-AuNP@Van. *C. albicans*: (a) DIC panel (b) red panel (propidium iodide), (c) blue emission (PEI-AuNP@Van), and (d) all merged panel. *C. tropicalis*; (e) DIC panel, (f) red emission panel (propidium iodide), (g) blue emission (PEI-AuNP@Van) panel, and (h) merged panel.

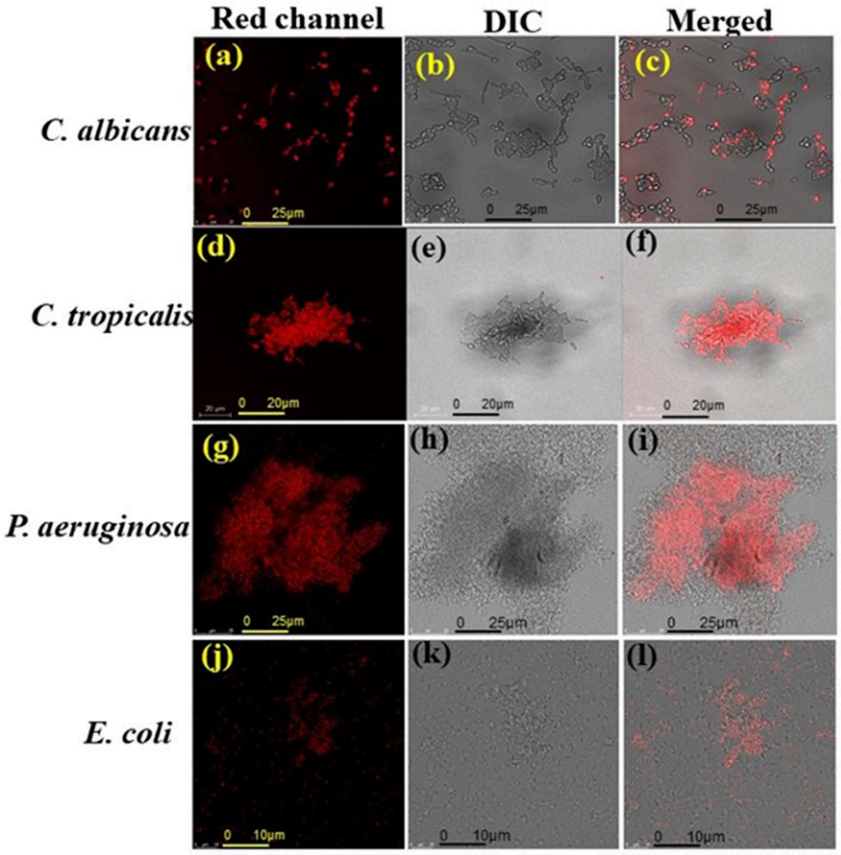

Figure 4. Confocal micrographs representing dead cells after the exposure to PEI-AuNP@Van for 4 h. *C. albicans* (a: PI emission panel; b: DIC panel and c: red, DIC merged panel); *C. tropicalis*, (d: PI emission panel; e: DIC panel and f: red, DIC merged panel); *E. coli* (g: PI emission panel; h: DIC panel and i: red, DIC merged panel) and *P. aeruginosa* (j: PI emission panel; k: DIC panel and l: red, DIC merged panel).

untreated growth control, the PEI-AuNP- and PEI-AuNP@Van-treated cells demonstrated a substantial increase in DCF fluorescence. After treatment with PEI-AuNP@Van *C. albicans* (11.38 %; Figure 6(a)), *C. tropicalis* (25.02 %; Figure 6(b)), *E. coli* (30.4%; Figure 6(c)), and *P. aeruginosa* (36.0 %; Figure 6(d)) populations demonstrated elevated endogenous reactive oxygen species as compared to PEI-AuNP and the standard drug control. In contrast, untreated control cells showed negligible ROS generation. These results justify the ROS induction activity of PEI-AuNP@Van in treated microbial cultures.

To assess whether PEI-AuNP@Van-treated *C. albicans, C. tropicalis, E. coli*, and *P. aeruginosa* cells exhibit apoptotic phenomena, annexin V-FITC/PI and confocal microscopy studies were performed. The results indicate that all treated microbial strains, except *C. albicans* (Figure 7(a)–(d))), displayed early and late apoptotic properties (as shown in Figure 7). Notably, *P. aeruginosa* (Figure 7(m)–(p)) showed significant apoptotic behavior, followed by *E. coli* (Figure 7(i)–(l)).

Raman spectroscopy analysis

Raman spectrometry of *C. albicans*, *C. tropicalis*, *E. coli*, and *P. aeruginosa* was performed after treatment with PEI-AuNP@Van; the recorded spectra matched and validated with previously reported Raman band fingerprints and molecular assignments; multivariate data analysis and mean spectral analysis were performed.[38–50]

Raman spectroscopy of C. albicans *and* C. tropicalis. Figure 8(a) and (d) show the Raman spectra that were obtained from untreated cells and PEI-AuNP@Van- and amphotericin B-treated *C. albicans* and *C. tropicalis* cells, respectively. In the untreated cells, Raman bands appeared at 487 cm^{-1} (CCO bending and COHO torsion in chitin), 531 cm^{-1} (CCC, β(CCO), OCO bending in chitin), and 539 cm^{-1}. Features at 726-735 cm^{-1} (CO stretching, ring deformation of glucosyl unit/adenine, and glycosides) were observed in both species. Bands at 808-810 cm^{-1} correspond to asymmetric OPO phosphodiester stretching; the 1040 cm^{-1} band is linked to C–C stretching

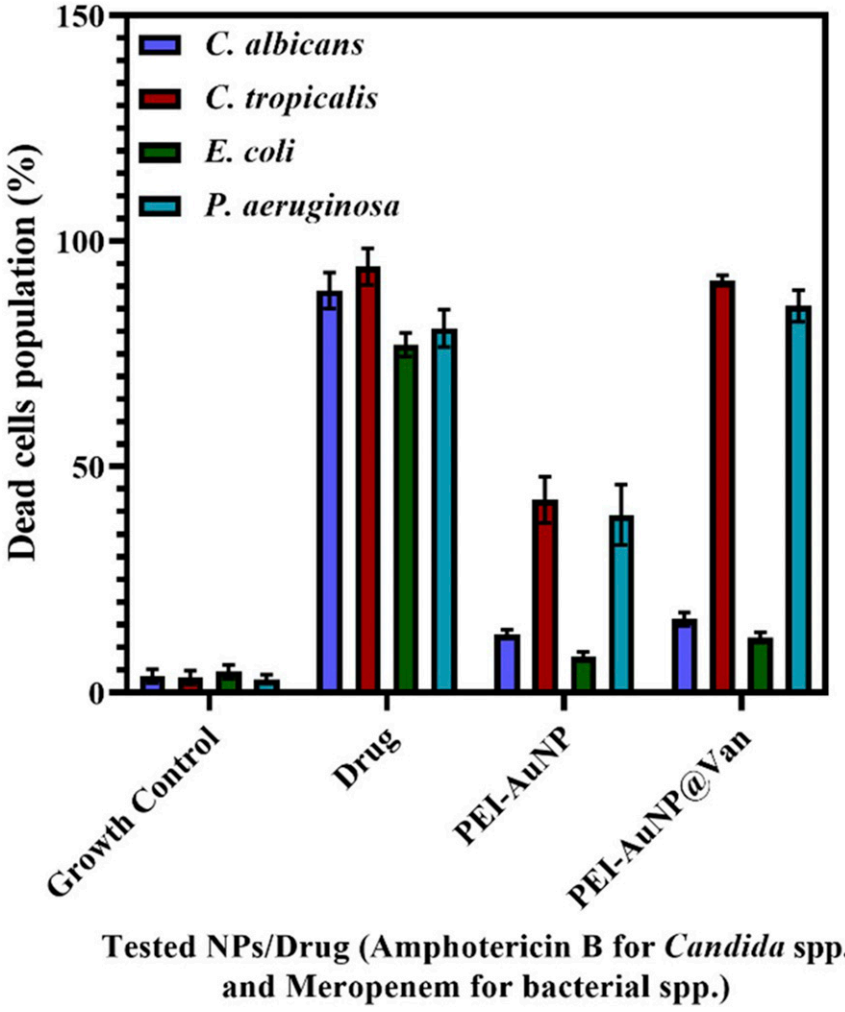

Figure 5. Graph representing dead cell populations after 4 h of exposure to PEI-AuNP@Van along with amphotericin B and meropenem (for *Candida* spp. And Gram-negative bacteria, respectively) and unconjugated PEI-AuNPs. Data are presented as mean values of three independent experimental replicates.

(phospholipids, chitin) and C–N stretching. The 1135 cm^{-1} band relates to = C–O–C= (unsaturated fatty acids in lipids), which is common to both species. The 1248 cm^{-1} band in *C. tropicalis* was linked to amide III (random) bonding and was absent in *C. albicans*. Both species showed bands at 1314 and 1323 cm^{-1} (amide III bonding, protein, or CH deformation), and CH_2 deformation bands at 1449 and 1452 cm^{-1}, respectively. The 1582 cm^{-1} band in *C. tropicalis* (absent in *C. albicans*) was attributed to NH_2 deformations/amide III of proteins; the 1663 cm^{-1} band, common to both, was linked to chitin. These peaks corresponded to the *Candida* cell wall components: mannoproteins, glucan, and chitin. The spectra of amphotericin B- and PEI-AuNP@Van-treated cells were compared with those of untreated cells to study the mode of action and structural changes of PEI-AuNP@Van. Differences were noted at 587 cm^{-1} (absent in *C. albicans*), 590 cm^{-1}, 676 cm^{-1}, 685 cm^{-1}, 852 cm^{-1} (absent in *C. albicans*), 914 cm^{-1}, 1125 cm^{-1}, 1162 cm^{-1}, 1214 cm^{-1} (absent in *C. albicans*), 1314 cm^{-1}, 1582 cm^{-1} (absent in *C. albicans*), 1602 cm^{-1}, and 1653 cm^{-1}. These features (Figure 8(a) and (d) and Supplement Table S1) are attributed to in-plane bending (CCC), β(CCO), and β(OCO) in chitin glycosidic linkage (587, 590 cm^{-1}); guanine and tyrosine (676 cm^{-1}); in-plane CCO bending in glucosyl unit (685 cm^{-1}, absent in *C. tropicalis*); CH_2 twisting, CC stretching in glucosyl unit (852 cm^{-1}), CC bond stretching (914 cm^{-1}, absent in *C. tropicalis*); C–O ring, aromatic amino acids in proteins (1162 cm^{-1}, absent in *C. tropicalis*), amide III (random), and thymine (1214 cm^{-1}, absent in *C. albicans*).

Raman spectroscopy analysis of E. coli *and* P. aeruginosa. Unlike fungal cells, Gram-negative bacteria exhibit a thin peptidoglycan cell wall that is enclosed by a

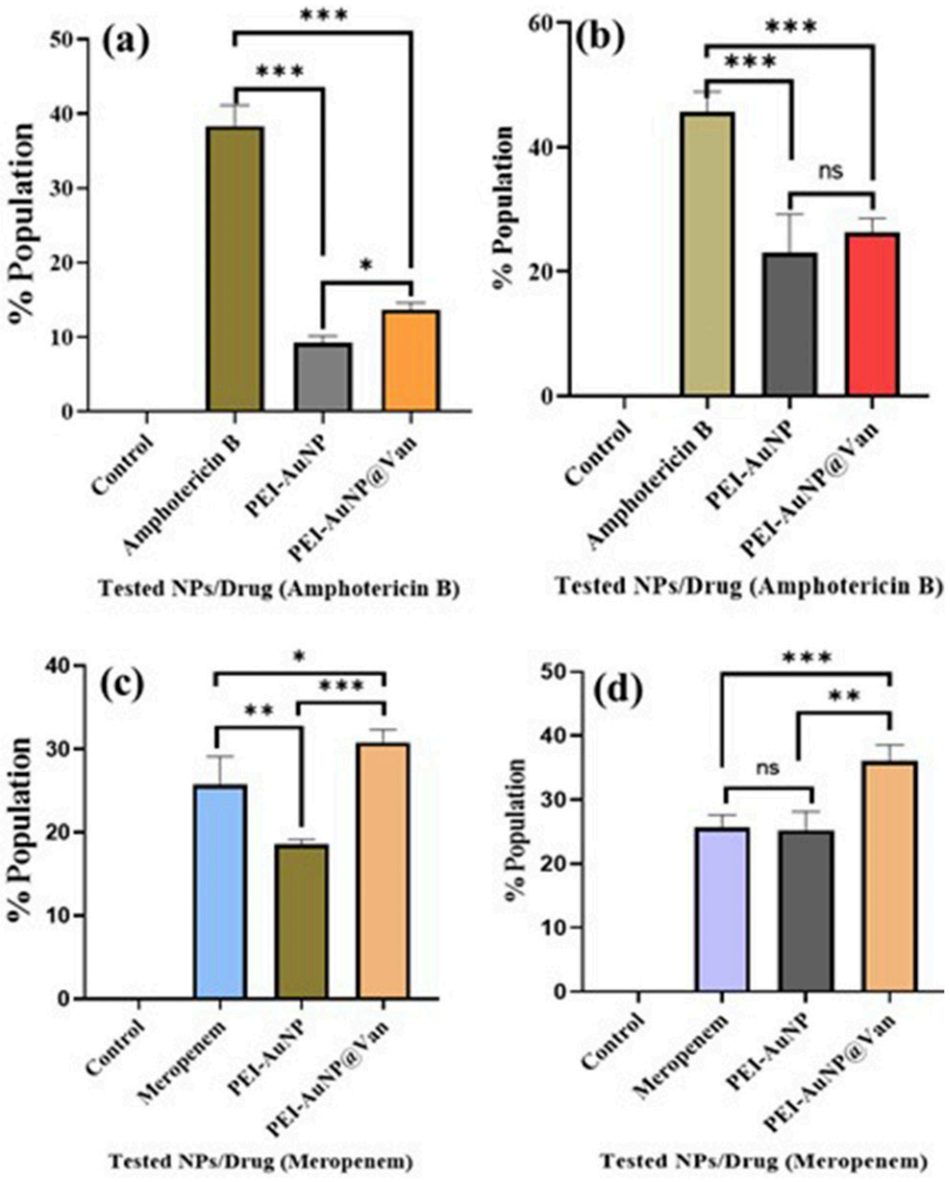

Figure 6. Graph representing endogenous ROS-accumulated populations of 4 h exposed cultures of tested microbial species with PEI-AuNP@Van along with drug and unconjugated PEI-AuNPs. (a) *C. albicans*; (b) C. *tropicalis*; (c) *E. coli*, and (d) *P. aeruginosa*. The data are described as the mean value of three independent experimental replicates, and an ordinary one-way ANOVA was completed to compare the tested variables (*p* value *** = <0.001; ** = 0.007; * = 0.04, and ns = > 0.05).

lipopolysaccharide outer membrane. Raman spectroscopy of untreated, PEI-AuNP@Van, and meropenem-treated *E. coli* and *P. aeruginosa* cells (Figure 8(c) and (d)) revealed weak and strong peaks between 400 and 1660 cm^{-1}. Peaks included 748 cm^{-1} (C–S (protein)/CH_2 rocking/adenine, peptidoglycan), 997 or 1002 cm^{-1} (in-plane (CH), Phe, (CC) aromatic ring, ring-breathing (CC) polysaccharides), 1122 or 1127 cm^{-1} (stretching (C–C) skeletal of acyl backbone in lipid), 1167 cm^{-1} (C–H in-plane bending in tyrosine, absent in *E. coli*), 1243 cm^{-1} (asymmetric phosphate stretching, amide III), 1311 cm^{-1} (CH_2 wagging and twisting), 1329 cm^{-1} (COH (mono, oligosaccharide) amide III, bend (CH), (OH) (polysaccharide) d (OH), in-plane (CH_2), 1341 cm^{-1} (amide III, Trp; bend (CH), d (OH) (polysaccharide), 1392-1404 cm^{-1} (symm (CO_2) alanine), 1450 cm^{-1} (CH_2) (fatty acid chains, phospholipids, amino side-chains of proteins); CH_3, CH_2, COH (mono or oligosaccharides), 1578-1585 cm^{-1} (νCOO−; C-C, N–H deformation; C–N stretching (amide II)), and 1658 cm^{-1} (amide I), indicating fingerprint bonds of untreated cells (Figure 8(c) and (d)). Comparison of treated *E. coli* and *P. aeruginosa* cells with

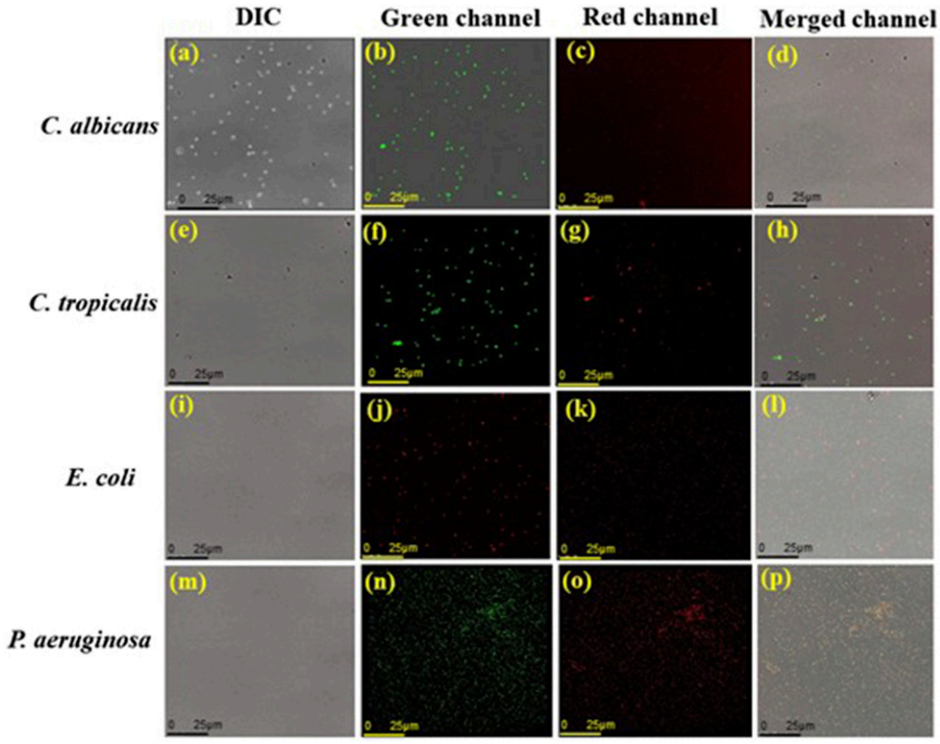

Figure 7. Confocal micrographs representing phosphatidylcholine externalization assay using the Annexin-V/PI staining system after 4 h exposure to PEI-AuNP@Van against microbial species. *C. albicans*: (a) DIC panel, (b) green panel (Annexin-V stained cells), (c) red panel (PI stained cells), and (d) all merged panel; *C. tropicalis*: (e) DIC panel, (f) green panel (Annexin-V stained cells), (g) red panel (PI stained cells), and (h) all merged panel); *E. coli*: (i) DIC panel, (j) green panel (Annexin-V stained cells), (k) red panel (PI stained cells), and (l) all merged panel); and *P. aeruginosa*: (m) DIC panel, (n) green panel (Annexin-V stained cells), (o) red panel (PI stained cells), and (p) all merged panel).

untreated controls showed spectral band differences (Figure 8(c) and (d)). Peaks at 534 cm^{-1}, 848 cm^{-1}, 1506 cm^{-1}, and 1600 cm^{-1} were absent in untreated *E. coli*, while 637 cm^{-1} and 1662 cm^{-1} were absent in *P. aeruginosa*. (Figure 8(c) and (d)).

Principle component analysis. The principal component analysis (PCA) of Raman spectral datasets for *C. albicans, C. tropicalis, E. coli*, and *P. aeruginosa* (Figure 8(b), (c), (e), (f), (h), (i), (k) and (l)) show three distinct clusters, each indicated by a different color, formed by the separation of Raman spectra. Each dot within a cluster represents a single spectrum, with clusters aligned along the positive axis of the first principal component (PC-1). These clusters represent spectral datasets for *candida* strains, *E. coli*, and *P. aeruginosa* exposed to PEI-AuNP@Van, amphotericin B, and meropenem, respectively, as well as untreated cells. PC-1 explained the largest data variability: 66.57% (Figure 8(b) and (c))), 93.02% (Figure 8(e) and (f))), 89.66% (Figure 8(h) and (i))), and 75.20% (Figure 8(k) and (l))) for *C. albicans, C. tropicalis, E. coli*, and *P. aeruginosa*, respectively, with PC-2 accounting for the remaining variability. PCA identified and verified distinctive Raman spectral features, showing that Raman spectroscopy could detect spectral changes owing to biochemical alterations induced by PEI-AuNP@Van in the exposed strains.

Ultrastructural (TEM) analysis

The TEM analysis revealed the cell complexity-dependent antimicrobial activity of PEI-AuNP@Van. Figure 9 demonstrates the cell wall-damaging action in *C. albicans* and *C. tropicalis* (Figure 9(a)–(d)). However, the selective surface binding was noted in *E. coli* and *P. aeruginosa* cells (Figure 9(e)–(h) yellow arrow). The results confirmed that the PEI-AuNP@Van surface interaction dynamics and mechanochemical impact were different for fungi and Gram-negative bacteria (as shown in Figure 9). Additionally, an intriguing observation was made in a few *E. coli* populations treated with PEI-AuNP@Van; numerous spherical structures with surface-attached nanoparticles were visible (Figure 10), suggesting an PEI-AuNP@Van-induced apoptotic phenomenon in bacterial strains.

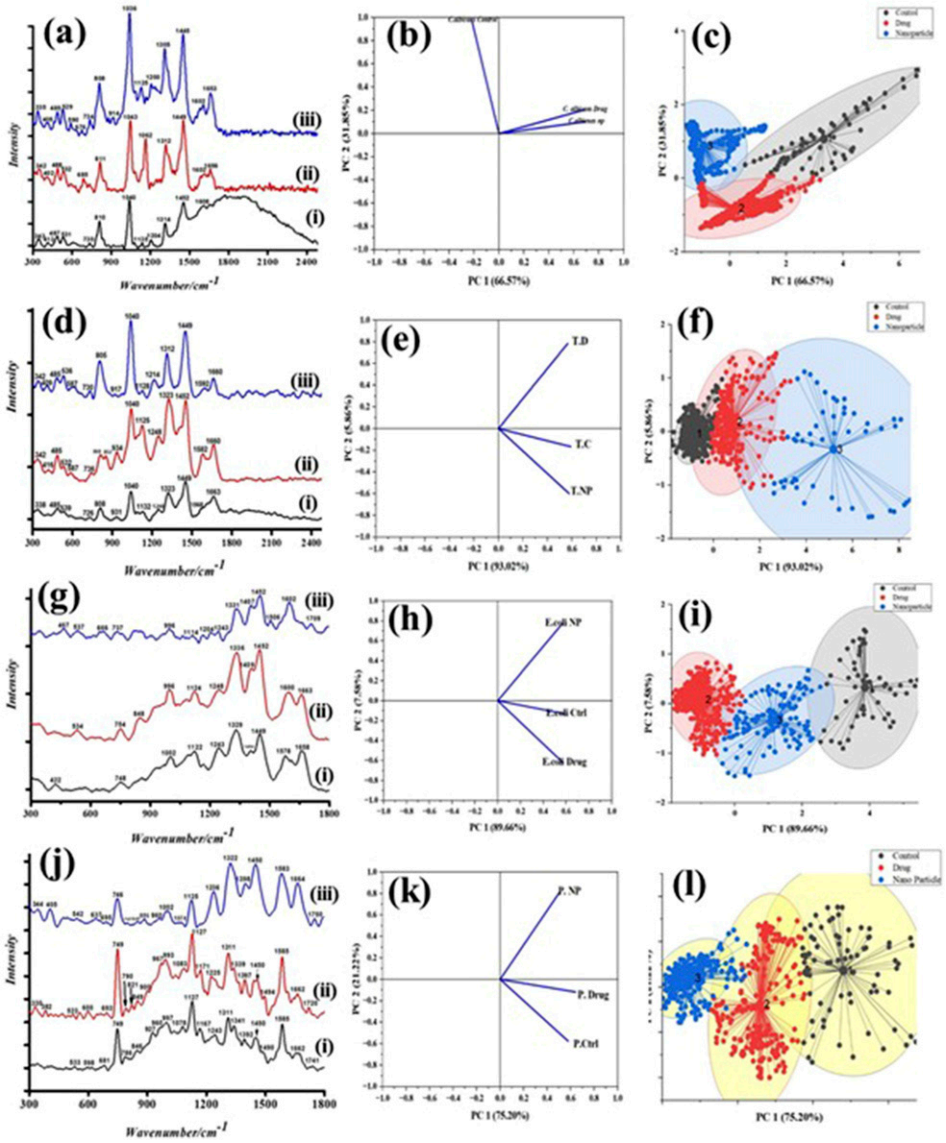

Figure 8. Raman spectra and PCA analysis of PEI-AuNP@Van treated microbial cells. (a) Raman spectrum of *C. albicans*: (i) untreated cell control, (ii) amphotericin B treated, and (iii) PEI-AuNP@Van treated. (b) Loading plot and (c) k-cluster plot. (d) Raman spectrum of *C. tropicalis*: (i) untreated cell control, (ii) amphotericin B treated, and (iii) PEI-AuNP@Van treated. (e) Loading plot and (f) k-cluster plot. (g) Raman spectrum of *E. coli*: (i) untreated cell control, (ii) meropenem-treated, and (iii) PEI-AuNP@Van-treated. (h) Loading plot and (i) k-cluster plot. (j) Raman spectrum of *P. aeruginosa*: (i) untreated growth control, (ii) meropenem treated, and (iii) PEI-AuNP@Van treated. (k) Loading plot and (l) k-cluster plot.

Cytotoxicity assay involving the HEK-293 cell line

The conventional MTT assay was utilized to investigate the mammalian cell cytotoxicity of the PEI-AuNP@Van nanosystem in cells from the Human Embryonic Kidney (HEK) 293 cell line. Specifically, HEK-293 cells were incubated with PEI-AuNP@Van at different concentrations; the results showed that PEI-AuNP@Van exhibited moderate concentration-dependent cytotoxicity (as demonstrated in Figure 11). PEI-AuNP@Van exhibited approximately 84% viability at a concentration of 10 µg/mL, whereas it had the highest cell toxicity (47%) at 100 µg/mL. These results indicate that PEI-AuNP@Van caused cell toxicity at higher concentrations.

Discussion

AuNPs are useful in medical applications such as imaging and drug delivery. They can be linked to large molecules, including antimicrobial drugs, via surface interactions. The growing issue of antimicrobial resistance and declining efficacy of current drugs pose a global health threat,

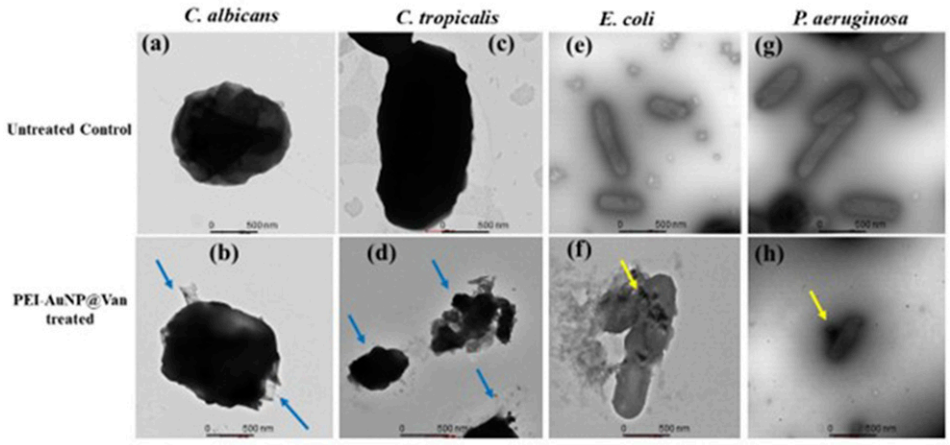

Figure 9. Transmission electron micrographs of PEI-AuNP@Van-exposed microbial strains and the respective untreated control cells. (a) untreated control cells of *C. albicans*, (b) treated with PEI-AuNP@Van, (c) untreated control cells of *C. tropicalis*, (d) treated with PEI-AuNP@Van, (e) untreated control cells of *E. coli*, (f) treated with PEI-AuNP@Van, (g) untreated control cells of *P. aeruginosa*, and (h) treated with PEI-AuNP@Van.

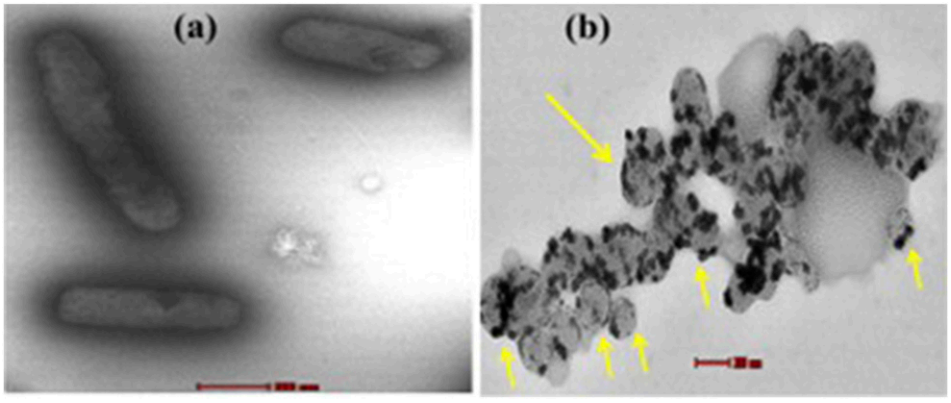

Figure 10. TEM micrographs of PEI-AuNP@Van treated *E. coli* cells showing apoptotic behavior; (a) cell control and (b) treated cell.

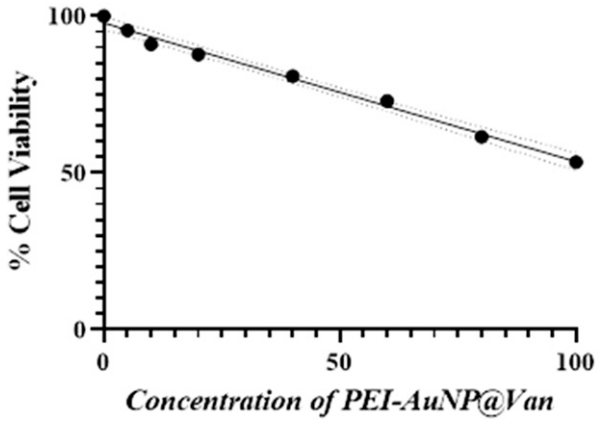

Figure 11. Biocompatibility of PEI-AuNP@Van particles against HEK cells.

necessitating new antimicrobial alternatives for infections caused by *Candida* spp. And Gram-negative bacteria. Our team optimized a rapid protocol for developing fluorescent vancomycin-conjugated gold nanoparticles (PEI-AuNP@Van); the prepared nano-system was explored for its antimicrobial applications.[32,33] In this system, vancomycin coordinates with gold cations and the NH- group of PEI interacts with the COO/OH groups of vancomycin via electrostatic interactions or hydrogen bonding, as confirmed by ATR-FTIR spectroscopy (Figure 2) and supported by Hagbani et al. 2022.[10] Further studies are required to fully understand these mechanisms. Vancomycin significantly affected the nanogeometry of PEI-AuNP@Van, resulting in the formation of spherical particles (<10 nm; Figure 1(d)). Electrostatic stability measurements using zeta potential studies revealed a high value (48 mV) at ambient

temperature (Figure 1(c)) due to non-equivalent vancomycin conjugation with PEI-AuNPs, which leads to slight polydispersity (4-12 nm; Figure 1(d)) and results in a bimodal distribution of the zeta potential. To validate

These findings, AFM was conducted to understand the morphology and polydispersion of PEI-AuNP@Van. The Z-axis data from this analysis clearly indicated that the nanoparticles were spherical, with an average diameter that ranged from 4 to 10 nm (Figure 1(f)). The size distribution observed between these two characterization techniques can be attributed to the increased likelihood of nanoparticle conjugation with the silanized surface during the AFM measurements. The intrinsic fluorescence of vancomycin made PEI-AuNP@Van highly luminescent and excitation-dependent (λex = 270–360 nm; λem = 420 nm) with a quantum yield of 15.40%, making the materials traceable under UV exposure.[32,33]

Vancomycin inhibits RNA synthesis by forming hydrogen bonds with NAM/NAG residues, preventing their incorporation into the peptidoglycan matrix.[51] The outer lipopolysaccharide (LPS) layer of Gram-negative bacteria obstructs vancomycin access to the peptidoglycan layer, making it ineffective. Yeast cell walls, composed of chitin, proteins, and mannoproteins, differ structurally from bacterial cell walls.[52] PEI-stabilized metal nanoparticles interact with bacterial and fungal cell surfaces via electrostatic forces, permeabilizing the LPS layer and permitting vancomycin to reach the peptidoglycan layer, leading to cell death.[53–56] PEI-AuNP@Van exhibited stronger antimicrobial effects against *Candida* spp. And Gram-negative bacteria than unconjugated PEI-AuNPs, while free vancomycin remained inactive (Table 1). *C. tropicalis* and *P. aeruginosa* were more sensitive to PEI-AuNP@Van compared to *C. albicans* and *E. coli* strains. Notably, *C. tropicalis* exhibited a significantly higher level of chitin than *C. albicans*. In contrast, the majority of *Candida* species showed similar levels of glucan in their cell walls, with *C. tropicalis* being the exception, demonstrating a markedly lower glucan content than *C. albicans*.[57] Hence, this cell wall structural variation probably led to the species-dependent mode of action of PEI-AuNP@Van. Cellular localization studies showed PEI-AuNP@Van inside *C. albicans* and *C. tropicalis* (Figure 3 and Supplement Figure S1), and on the surfaces of *E. coli* and *P. aeruginosa*, again indicating selective binding and antimicrobial action based on structural differences. High cell membrane integrity loss was observed in *C. tropicalis* (91.8%) and *P. aeruginosa* (85.8%) using propidium iodide staining and dead cell enumeration (Figures 4 and 5), while *C. albicans* and *E. coli* exhibited slower death rates after 4 h of exposure to PEI-AuNP@Van at MIC values. Unconjugated PEI-AuNPs also significantly killed *C. albicans* and *E. coli* strains, indicating a minimal role of vancomycin. Additional investigations are necessary to fully understand the species-specific mode of action of PEI-AuNP@Van.

The action of PEI-AuNP@Van on various strains was evaluated using assays and imaging techniques including ROS accumulation, apoptosis assays, Raman spectroscopy, and TEM. While essential for cellular functions, excessive ROS causes oxidative stress, leading to apoptosis or necrosis.[58,59] Flow cytometry with DCFH-DA staining revealed cell type-dependent ROS induction profiles in treated strains (Figure 6 and Supplement Figure S3). PEI-AuNPs and PEI-AuNP@Van induced similar ROS levels in *C. albicans* and *C. tropicalis*, suggesting that vancomycin reduced ROS production (Figure 6(b)). However, ROS accumulation alone did not fully explain the PEI-AuNP@Van activity relative to the total dead population (Figure 5).[59] To explore alternative mechanisms, an apoptosis assay using annexin V-FITC/PI staining was performed. AuNPs are known to penetrate cell membranes and induce apoptosis-like death (including DNA damage, membrane depolarization, and caspase-like protein activation) in fungi and Gram-negative bacteria without increasing ROS levels.[59] Thus, multiple programmed cell death mechanisms may vary with microbial diversity.[60] During early apoptosis, phosphatidylserine translocates from the inner leaflet to the outer leaflet of the plasma membrane.[61,62] Annexin V then binds to this externalized phosphatidylserine when in the presence of Ca^{2+} ions. In this double-staining approach, the early apoptotic cells were stained only by annexin V-FITC; necrotic and late apoptotic cells were stained by both PI and annexin V-FITC. An apoptosis assay using annexin V-FITC/PI staining investigated other mechanisms, as AuNPs can induce apoptosis-like death in fungi and Gram-negative bacteria without increasing ROS levels.[59] PEI-AuNP@Van-treated *C. albicans* cells exhibited early apoptosis properties (Figure 7(a)–(d)), while *C. tropicalis*, *E. coli*, and *P. aeruginosa* showed both early and late apoptotic/necrotic behavior (Figure 7(e)–(p)). This suggests ROS-independent apoptosis and cell death in *C. albicans*,[63] whereas *C. tropicalis*, *E. coli* (Figure 10), and *P. aeruginosa* undergo ROS-induced apoptosis, indicating multiple modes of action for PEI-AuNP@Van depending on the cell type.

Raman spectroscopy can be utilized to understand chemical bonding in biological macromolecules after interaction with metal nanoparticles, revealing significant structural and compositional changes in cells, including modifications of the nucleic acid phosphate backbone, disrupted protein hydrogen bonds, and reduced lipid molecule stacking forces.[64] In treated *C. albicans*, Raman bands shifting at 590, 676, 914, 1125, 1314, 1602, and 1653 cm^{-1} indicated alterations in chitin and unsaturated lipid chains (Figure 8(a)–(c)); this result was confirmed by TEM analysis showing damaged cell walls (Figure 9(a) and (b)). *C. tropicalis* exhibited similar Raman shifts at 526, 587, 852, 917, 1312, and 1592 cm^{-1}, suggesting changes in

chitin, lipid, and protein structures (Figure 8(d)–(f)), with complete cellular rupture observed under TEM (Figure 9(c) and (d)); this finding may be potentially due to excessive ROS accumulation, leading to cellular collapse.[65] *E. coli* and *P. aeruginosa*, despite similar cellular compositions, exhibit molecular differences in their Raman spectra (Figure 8(g) and (j)). Untreated *E. coli* (i), meropenem-treated (ii), and PEI-AuNP@Van-treated cells (iii) display peaks at 530-550 cm^{-1} and 848 cm^{-1}, which correspond to peptidoglycan deformation and various molecular vibrations. Glycosidic linkage deformation supports the action of vancomycin, and spectral changes (e.g., a peak shift from 1122 cm^{-1} to 1114 cm^{-1}) indicate membrane lipid and carbohydrate stretching[66]; these findings are aligned with TEM images of peptidoglycan sheet fractures (Figure 9(e) and (f)). *P. aeruginosa* showed no significant Raman band shifts between treatments (Figure 8(j)), with minor changes at 533 cm^{-1} to 542 cm^{-1} and 786 cm^{-1} to 797 cm^{-1}, which were related to peptidoglycan and lipid stretching. TEM revealed no cellular fracture in *P. aeruginosa*; however, PEI-AuNP@Van nanoparticles were adsorbed on the cell surface (Figure 9(g) and (h)). Additionally, an intriguing observation was made in a few *E. coli* populations treated with PEI-AuNP@Van; numerous spherical structures with surface-attached nanoparticles were visible (Figure 10), suggesting an PEI-AuNP@Van-induced apoptotic phenomenon in bacterial strains.

Conclusions

Vancomycin-conjugated PEI-stabilized gold nanoparticles (PEI-AuNP@Van) were synthesized and evaluated for antimicrobial activity against *C. albicans, C. tropicalis, E. coli*, and *P. aeruginosa*, along with their modes of action. PEI-AuNP@Van showed significant antimicrobial effects within 4 h, with MIC values of 4.8 µg/mL for *C. albicans*, 1.2 µg/mL for *C. tropicalis*, 2.5 µg/mL for *E. coli*, and 4.81 µg/mL for *P. aeruginosa*. These nanoparticles emitted blue fluorescence (418-430 nm), facilitating tracking of intracellular localization in *C. albicans and C. tropicalis*, and adsorption on *E. coli* and *P. aeruginosa* surfaces. Viability assays revealed that 16.3% of *C. albicans*, 91.8% of *C. tropicalis*, 12% of *E. coli*, and 85.8% of *P. aeruginosa* populations were killed within 4 h of treatment. PEI-AuNP@Van-treated cells accumulated endogenous ROS in 11.38% of *C. albicans*, 25.02% of *C. tropicalis*, 30.4% of *E. coli*, and 36.0% of *P. aeruginosa* populations. Phosphatidylcholine externalization indicated apoptosis-like behavior in all strains, with fungal strains showing early apoptosis. Raman spectroscopy and TEM analysis revealed multiple modes of action: ROS-dependent and independent apoptosis and cell wall damage in *C. albicans* and *C. tropicalis*, and ROS-induced apoptosis and peptidoglycan sheet deterioration in *E. coli* and *P. aeruginosa*. PEI-AuNP@Van nanoparticles effectively targeted a broad range of pathogenic microorganisms. However, comprehensive biocompatibility evaluations (both in vitro and in vivo) are essential. The efficacy of the PEI-AuNP@Van nanoparticles against planktonic cells has been documented, but their effectiveness against biofilms of mono- or mixed-species remains to be studied.

Acknowledgments

The authors would like to thank the Central Instrument Facility, Indian Institute of Technology (BHU), for characterization of the nanoparticles, the Central Discovery Centre (CDC), Banaras Hindu University, for providing access to flow cytometry and Raman spectroscopy, and SATHI BHU for laser scanning super-resolution microscopy. The authors also thank SAIF, AIIMS, New Delhi, India, for TEM imaging of biological samples.

Authors Contribution

AN and AKT contributed equally. Conceptualization: AKT and MKG; Data curation: AKT; Formal analysis: AKT; Funding acquisition: MKG and RJN; Investigation: AN and AKT; Methodology: AN, AKT and MKG; Project administration: MKG and RJN; Resources: MKG, AC & PCP; Software: AKT; Supervision: PCP, and RJN; Validation: AKT and MKG; Visualization: AN, AKT and MKG; Roles/Writing - original draft: AKT; Writing - review and editing: AKT and RJN. All of the authors reviewed and agreed to this submission.

Declaration of Conflicting Interests

The author(s) declared no potential conflicts of interest with respect to the research, authorship, and/or publication of this article.

Funding

The author(s) disclosed receipt of the following financial support for the research, authorship, and/or publication of this article: This work is partially supported by an Incentive Grant under IoE to Dr. MK Gupta (R/Dev/D/IoE/seed & Incentive grant_III/2022-23/49235).

ORCID iD

Roger J. Narayan https://orcid.org/0009-0001-8765-8395

Supplemental Material

Supplemental material for this article is available online.

References

1. Nami S, Mohammadi R, Vakili M, et al. Fungal vaccines, mechanism of actions and immunology: a comprehensive review. *Biomed Pharmacother* 2019; 109: 333–344.

2. Medici NP and Del Poeta M. New insights on the development of fungal vaccines: from immunity to recent challenges. *Mem Inst Oswaldo Cruz* 2015; 110: 966–973.
3. Sakagami T, Kawano T, Yamashita K, et al. Antifungal susceptibility trend and analysis of resistance mechanism for Candida species isolated from bloodstream at a Japanese university hospital. *J Infect Chemother* 2019; 25(1): 34–40.
4. Spampinato C and Leonardi D. Candida infections, causes, targets, and resistance mechanisms: traditional and alternative antifungal agents. *BioMed Res Int* 2013; 2013(1): 204237.
5. Cheng MF, Yang YL, Yao TJ, et al. Risk factors for fatal candidemia caused by Candida albicans and non-albicans Candida species. *BMC Infect Dis* 2005; 5: 22.
6. Pahwa N, Kumar R, Nirkhiwale S, et al. Species distribution and drug susceptibility of Candida in clinical isolates from a tertiary care centre at Indore. *Indian J Med Microbiol* 2014; 32(1): 44–48.
7. Murray CJ, Ikuta KS, Sharara F, et al. Global burden of bacterial antimicrobial resistance in 2019: a systematic analysis. *The lancet* 2022; 399(10325): 629–655.
8. Davies SC, Fowler T, Watson J, et al. Annual report of the chief medical officer: infection and the rise of antimicrobial resistance. *Lancet* 2013; 381(9878): 1606–1609.
9. Laxminarayan R, Sridhar D, Blaser M, et al. Achieving global targets for antimicrobial resistance. *Science* 2016; 353(6302): 874–875.
10. Hagbani TA, Yadav H, Moin A, et al. Enhancement of vancomycin potential against pathogenic bacterial strains via gold nano-formulations: a nano-antibiotic approach. *Materials* 2022; 15(3): 1108.
11. Rizvi SMD, Lila ASA, Moin A, et al. Antibiotic-loaded gold nanoparticles: a nano-arsenal against ESBL producer-resistant pathogens. *Pharmaceutics* 2023; 15(2): 430.
12. Mitchell MJ, Billingsley MM, Haley RM, et al. Engineering precision nanoparticles for drug delivery. *Nat Rev Drug Discov* 2021; 20(2): 101–124.
13. Blanco E, Shen H and Ferrari M. Principles of nanoparticle design for overcoming biological barriers to drug delivery. *Nat Biotechnol* 2015; 33(9): 941–951.
14. Shabatina T, Vernaya O, Shumilkin A, et al. Nanoparticles of bioactive metals/metal oxides and their nanocomposites with antibacterial drugs for biomedical applications. *Materials* 2022; 15(10): 3602.
15. Khorsandi K, Hosseinzadeh R, Sadat Esfahani H, et al. Nanomaterials as drug delivery systems with antibacterial properties: current trends and future priorities. *Expert Rev Anti Infect Ther* 2021; 19(10): 1299–1323.
16. Kotrange H, Najda A, Bains A, et al. Metal and metal oxide nanoparticle as a novel antibiotic carrier for the direct delivery of antibiotics. *Int J Mol Sci* 2021; 22(17): 9596.
17. Klębowski B, Depciuch J, Parlińska-Wojtan M, et al. Applications of noble metal-based nanoparticles in medicine. *Int J Mol Sci* 2018; 19(12): 4031.
18. Monti S, Jose J, Sahajan A, et al. Structure and dynamics of gold nanoparticles decorated with chitosan–gentamicin conjugates: ReaxFF molecular dynamics simulations to disclose drug delivery. *Phys Chem Chem Phys* 2019; 21(24): 13099–13108.
19. Wang S, Yan C, Zhang X, et al. Antimicrobial peptide modification enhances the gene delivery and bactericidal efficiency of gold nanoparticles for accelerating diabetic wound healing. *Biomater Sci* 2018; 6(10): 2757–2772.
20. Nawaz A, Ali SM, Rana NF, et al. Ciprofloxacin-loaded gold nanoparticles against antimicrobial resistance: an in vivo assessment. *Nanomaterials* 2021; 11(11): 3152.
21. Huang Z, Liu H, Zhang X, et al. Ceftazidime-decorated gold nanoparticles: a promising strategy against clinical ceftazidime-avibactam-resistant enterobacteriaceae with different resistance mechanisms. *Antimicrob Agents Chemother* 2023; 67(7): e0026223.
22. Park J, Shin E, Yeom JH, et al. Gold nanoparticle-DNA aptamer-assisted delivery of antimicrobial peptide effectively inhibits Acinetobacter baumannii infection in mice. *J Microbiol* 2022; 60(1): 128–136.
23. Rad MR, Kazemian H, Yazdani F, et al. Antibacterial activity of gold nanoparticles conjugated by aminoglycosides against A. baumannii isolates from burn patients. *Recent Pat Anti-Infect Drug Discov* 2018; 13(3): 256–264.
24. Yeom JH, Lee B, Kim D, et al. Gold nanoparticle-DNA aptamer conjugate-assisted delivery of antimicrobial peptide effectively eliminates intracellular Salmonella enterica serovar Typhimurium. *Biomaterials* 2016; 104: 43–51.
25. Mu W, Fang W and Yao Y. Synthesis of Ag@ Au core–shell NPs loaded with ciprofloxacin as enhanced antimicrobial properties for the treatment and nursing care of Escherichia coli infection. *Microb Pathog* 2021; 150: 104619.
26. Shaker MA and Shaaban MI. Formulation of carbapenems loaded gold nanoparticles to combat multi-antibiotic bacterial resistance: in vitro antibacterial study. *Int J Pharm* 2017; 525(1): 71–84.
27. Rahimi H, Roudbarmohammadi S, Delavari H H, et al. Antifungal effects of indolicidin-conjugated gold nanoparticles against fluconazole-resistant strains of Candida albicans isolated from patients with burn infection. *Int J Nanomed* 2019; 14: 5323–5338.
28. Hsu LH, Wang HF, Sun PL, et al. The antibiotic polymyxin B exhibits novel antifungal activity against Fusarium species. *Int J Antimicrob Agents* 2017; 49(6): 740–748.
29. Zhai B and Lin X. Evaluation of the anticryptococcal activity of the antibiotic polymyxin B in vitro and in vivo. *Int J Antimicrob Agents* 2013; 41(3): 250–254.
30. Afeltra J and Verweij PE. Antifungal activity of nonantifungal drugs. *Eur J Clin Microbiol Infect Dis* 2003; 22: 397–407.
31. Isnard C, Hernandez SB, Guérin F, et al. Unexpected cell wall alteration-mediated bactericidal activity of the antifungal caspofungin against vancomycin-resistant Enterococcus

faecium. *Antimicrob Agents Chemother* 2020; 64(10): 10–1128.
32. Tiwari AK, Yadav HP, Gupta MK, et al. Synthesis of vancomycin functionalized fluorescent gold nanoparticles and selective sensing of mercury (II). *Front Chem* 2023; 11: 1238631.
33. Tiwari AK, Gupta MK, Yadav HP, et al. Aggregation-resistant, turn-on-off fluorometric sensing of glutathione and nickel (II) using vancomycin-conjugated gold nanoparticles. *Biosensors* 2024; 14(1): 49.
34. Zelazny AM, Ferraro MJ, Glennen A, et al. Selection of strains for quality assessment of the disk induction method for detection of inducible clindamycin resistance in staphylococci: a CLSI collaborative study. *J Clin Microbiol* 2005; 43(6): 2613–2615.
35. Chen J, Peng H, Wang X, et al. Graphene oxide exhibits broad-spectrum antimicrobial activity against bacterial phytopathogens and fungal conidia by intertwining and membrane perturbation. *Nanoscale* 2014; 6(3): 1879–1889.
36. Yadav S, Singh AK, Agrahari AK, et al. Making of water soluble curcumin to potentiate conventional antimicrobials by inducing apoptosis-like phenomena among drug-resistant bacteria. *Sci Rep* 2020; 10(1): 14204.
37. Nikhil A, Tiwari AK, Tilak R, et al. Vancomycin-conjugated polyethyleneimine-stabilized gold nanoparticles attenuate germination and show potent antifungal activity against Aspergillus spp. *Appl Sci* 2024; 14(16): 6926.
38. Wu X, Huang YW, Park B, et al. Differentiation and classification of bacteria using vancomycin functionalized silver nanorods array based surface-enhanced Raman spectroscopy and chemometric analysis. *Talanta* 2015; 139: 96–103.
39. Witkowska E, Korsak D, Kowalska A, et al. Strain-level typing and identification of bacteria–a novel approach for SERS active plasmonic nanostructures. *Anal Bioanal Chem* 2018; 410: 5019–5031.
40. Zając A, Hanuza J, Wandas M, et al. Determination of N-acetylation degree in chitosan using Raman spectroscopy. *Spectrochim Acta Mol Biomol Spectrosc* 2015; 134: 114–120.
41. De Gelder J, De Gussem K, Vandenabeele P, et al. Reference database of Raman spectra of biological molecules. *J Raman Spectrosc* 2007; 38(9): 1133–1147.
42. Freire PT, Barboza FM, Lima JA, et al. Raman spectroscopy of amino acid crystals. *Raman Spectroscopy and Applications* 2017; 201: 171.
43. Xia J, Li W, Sun M, et al. Application of SERS in the detection of fungi, bacteria and viruses. *Nanomaterials* 2022; 12(20): 3572.
44. Raza A, Parveen S, Majeed MI, et al. Surface-enhanced Raman spectral characterization of antifungal activity of selenium and zinc based organometallic compounds. *Spectrochim Acta Mol Biomol Spectrosc* 2023; 285: 121903.
45. Witkowska E, Jagielski T, Kamińska A, et al. Detection and identification of human fungal pathogens using surface-enhanced Raman spectroscopy and principal component analysis. *Anal Methods* 2016; 8(48): 8427–8434.
46. Hu H, Wang J, Yi X, et al. Stain-free Gram staining classification of pathogens via single-cell Raman spectroscopy combined with machine learning. *Anal Methods* 2022; 14(40): 4014–4020.
47. Sujith A, Itoh T, Abe H, et al. Imaging the cell wall of living single yeast cells using surface-enhanced Raman spectroscopy. *Anal Bioanal Chem* 2009; 394: 1803–1809.
48. Assmann C, Kirchhoff J, Beleites C, et al. Identification of vancomycin interaction with Enterococcus faecalis within 30 min of interaction time using Raman spectroscopy. *Anal Bioanal Chem* 2015; 407: 8343–8352.
49. Neugebauer U, Rösch P, Schmitt M, et al. On the way to nanometer-sized information of the bacterial surface by tip-enhanced Raman spectroscopy. *ChemPhysChem* 2006; 7(7): 1428–1430.
50. Colniță A, Dina NE, Leopold N, et al. Characterization and discrimination of gram-positive bacteria using Raman spectroscopy with the aid of principal component analysis. *Nanomaterials* 2017; 7(9): 248.
51. Mühlberg E, Umstätter F, Kleist C, et al. Renaissance of vancomycin: approaches for breaking antibiotic resistance in multidrug-resistant bacteria. *Can J Microbiol* 2020; 66(1): 11–16.
52. Watanakunakorn C. Mode of action and in-vitro activity of vancomycin. *J Antimicrob Chemother* 1984; 14 Suppl D(-suppl_D): 7–18.
53. Gow NA, Latge JP and Munro CA. The fungal cell wall: structure, biosynthesis, and function. *Microbiol Spectr* 2017; 5(3): 10–1128.
54. Tiwari AK, Gupta MK, Pandey G, et al. Molecular weight of polyethylenimine-dependent transfusion and selective antimicrobial activity of functional silver nanoparticles. *J Mater Res* 2020; 35(18): 2405–2415.
55. Tiwari AK, Gupta MK, Pandey G, et al. Size and zeta potential clicked germination attenuation and anti-sporangiospores activity of PEI-functionalized silver nanoparticles against COVID-19 associated Mucorales (Rhizopus arrhizus). *Nanomaterials* 2022; 12(13): 2235.
56. Tiwari AK, Gupta MK, Narayan RJ, et al. A whole cell fluorescence quenching-based approach for the investigation of polyethyleneimine functionalized silver nanoparticles interaction with Candida albicans. *Front Microbiol* 2023; 14: 1131122.
57. Walker LA and Munro CA. Caspofungin induced cell wall changes of Candida species influences macrophage interactions. *Front Cell Infect Microbiol* 2020; 10: 164.
58. Shaikh S, Rizvi SMD, Shakil S, et al. Synthesis and characterization of cefotaxime conjugated gold nanoparticles and their use to target drug-resistant CTX-M-producing bacterial pathogens. *J Cell Biochem* 2017; 118(9): 2802–2808.
59. Luo L, Huang W, Zhang J, et al. Metal-based nanoparticles as antimicrobial agents: a review. *ACS Appl Nano Mater* 2024; 7(3): 2529–2545.

60. Yang C, Jiang L, Zhang H, et al. Analysis of hypoxia-induced metabolic reprogramming. *Methods Enzymol* 2014; 542: 425–455.
61. Lee H and Lee DG. Gold nanoparticles induce a reactive oxygen species-independent apoptotic pathway in Escherichia coli. *Colloids Surf B Biointerfaces* 2018; 167: 1–7.
62. Nagamalleswari E, Rao S, Vasu K, et al. Restriction endonuclease triggered bacterial apoptosis as a mechanism for long time survival. *Nucleic Acids Res* 2017; 45(14): 8423–8434.
63. Dwyer DJ, Camacho DM, Kohanski MA, et al. Antibiotic-induced bacterial cell death exhibits physiological and biochemical hallmarks of apoptosis. *Mol Cell* 2012; 46(5): 561–572.
64. Tian EK, Wang Y, Ren R, et al. Gold nanoparticle: recent progress on its antibacterial applications and mechanisms. *J Nanomater* 2021; 2021(1): 1–18.
65. Lee B and Lee DG. Synergistic antibacterial activity of gold nanoparticles caused by apoptosis-like death. *J Appl Microbiol* 2019; 127(3): 701–712.
66. Pezzotti G. Raman spectroscopy in cell biology and microbiology. *J Raman Spectrosc* 2021; 52(12): 2348–2443.

Appendix

Abbreviations

PEI-AuNPs	Polyethyleneimine stabilized gold nanoparticles
PEI-AuNP@Van	Vancomycin conjugated polyethyleneimine stabilized gold nanoparticle
Van	Vancomycin
MIC	Minimum inhibitory concentration
PEI	Polyethyleneimine
μg	Microgram
mL	Microliter
AgNPs	Silver nanoparticles
AuNPs	Gold nanoparticles
LPS	Lipopolysaccharide
TEM	Transmission electron microscopy
DLS	Dynamic light scattering
XRD	X-Ray Diffraction
NAM/NAG	N-acetylmuramic acid (NAM) and N-acetylglucosamine (NAG)
λex/ λem	Excitation/emission wavelength